The following publication A. Belqorchi, U. Karaagac, J. Mahseredjian and I. Kamwa, "Standstill Frequency Response Test and Validation of a Large Hydrogenerator," in IEEE Transactions on Power Systems, vol. 34, no. 3, pp. 2261-2269, May 2019 is available at https://dx.doi.org/10.1109/TPWRS.2018.2889510.

Standstill Frequency Response Test and Validation of a Large Hydrogenerator

A. Belqorchi, *Member, IEEE,* U. Karaagac, *Member, IEEE,* J. Mahseredjian, *Fellow, IEEE,* I. Kamwa, *Fellow, IEEE*

***Abstract*— This paper intends to contribute to the revision process of the IEEE standard 115 by demonstrating the applicability of the Standstill Frequency Response (SSFR) test on large salient pole hydrogenerators. The presented SSFR tests are carried out on a 55.6 MVA salient pole machine with laminated rotor, non-continuous damper windings and a nonintegral slot number. The IEEE-115 SSFR test procedure is applied with special care to rotor positioning as well as accurate data acquisition in the low frequency range. The maximum likelihood estimation (MLE) method is utilized for machine parameter identification from the SSFR tests. Obtained parameters are compared with design values in addition to the ones obtained using traditional "sudden no-load three-phase short-circuit", Dalton-Cameron and "open stator d-axis transient time constant" methods. The accuracy of parameters is also confirmed by comparing the measured three-phase short-circuit current waveforms with the ones obtained by simulating the SSFR based machine models in an EMT-type software. Unlike to previous SSFR test cases on large salient pole hydrogenerators, accurate results are obtained.**

***Index Terms*— Equivalent circuits, frequency response, hydrogenerator, operational parameters, parameter determination, salient pole, synchronous machine.**

I. Introduction

HYDRO-QUÉBEC has been using some of the conventional tests described in the IEEE-115-2009 [1] standard for determining synchronous machine electrical parameters. Those tests include the "sudden no-load three-phase short-circuit" test, in which the machine is operating open-circuited at rated speed. The short-circuit test is essential in the commissioning stage for demonstrating the adequacy of the mechanical design of the machine to withstand the mechanical stresses arising from short circuit currents. It also enables to determine the second order d-axis model of the machine. However, it is risky to apply short-circuit tests to old machines for identifying or updating machine parameters, as they may not be able to withstand the harshness of such tests. Moreover, performing short-circuit tests in small power plants is a challenging task due to large space requirements for the short-circuit breaker and its accessories. In addition, the setup for sudden no-load three-phase short-circuit tests is time consuming and costly in general, especially for brushless machines.

The Standstill Frequency Response (SSFR) test has been developed as an alternative to traditional tests. Such test procedures are described in Section 12 of [1]. They basically involve exciting the stator or the field of the machine when the machine is offline and at standstill. The operational parameters of the machine, which are required to derive the complete model, can be obtained from the SSFR test results. These tests enable to obtain not only the d-axis, but also the q-axis models of the machine with an order of higher than two. Moreover, these tests can be performed either in the factory or at site and at a relatively low cost. On the other hand, SSFR testing is not common due to lack of accurate results for demonstrating its validity. Besides, SSFR testing is often believed to provide a model adequate only for small perturbations [2], and unable to produce information for the damper windings with small time constants due to the small signal to noise ratio [3].

The majority of available SSFR tests in the literature focus on turbo-generators [2], [4]-[7]. In [8], several SSFR test cases are presented and the distinctive characteristics of salient pole synchronous machines (SPSMs) from turbo-generators of round rotor construction, are revealed. Accurate rotor positioning and data acquisition in the low frequency range, are challenging issues for SSFR testing of SPSMs [8]. The measurement accuracy problem at low frequency is also apparent in [9]-[11] as the measured operational inductances exhibit scattered data and a slope instead of a clear horizontal asymptote at the origin.

Highest possible measurement accuracy is required at very low frequencies to circumvent the poor signal-to-noise ratio resulting from the typical low value of dc armature resistance [8]. Moreover, precise determination of the armature dc resistance is essential for the low frequency test. As the tests require several hours to complete at very low frequencies, it is essential to record the armature winding temperature throughout the tests, to correct the resistance values for any temperature variation [8]. Another alternative to avoid the inaccuracies resulting from temperature variations, is to reduce SSFR testing time using broadband excitation and measurement methods [12]-[14]. The significant sensitivity of operational inductances to noise and armature resistance is also demonstrated in [15].

With all the developed tools and gained experience over the

A. Belqorchi is with Hydro-Québec, Montréal, QC, Canada;
U. Karaagac is with Hong Kong Polytechnic University, Hong Kong, China;
J. Mahseredjian is with Polytechnique Montréal, Montréal, QC, Canada;
I. Kamwa is with IREQ, Varennes, QC, Canada.

years, the basic difficulties emphasized in [8] remain challenging issues [16]-[18]. Moreover, the majority of recent SSFR experiments and new techniques were conducted mainly on small or special laboratory machines. Due to small size, sometimes the required frequency range starts from higher than 0.005 Hz (such as in [19] and [20]) instead of the demanding very low frequency of 0.001 Hz. As the measurement current is often not negligible compared with the rated current, the signal-to-noise ratio is much higher than the one in large machines. If we add to that the fact that damper contact resistances are less sensitive to rotation, better SSFR data accuracy can be expected for small machines.

This paper contributes to the literature with a successful SSFR test experiment on a 55.6 MVA, 13.8 kV, 60 Hz, SPSM with 84 poles, 396 slots, laminated rotor iron and non-continuous damper windings. During SSFR tests, a sophisticated frequency response analyzer is used. Its gain accuracy is similar to [21], but it has better phase accuracy (0.02^0 instead of 0.1^0). In addition, the power amplifier is selected to be capable to supply constant currents to the stator in the range of dc to 20 Hz as the d- and q-axis operational inductances are affected by current levels at low frequencies.

Parameter identification from SSFR tests is achieved using the maximum likelihood estimation (MLE) method, described in [22]-[24]. The obtained machine parameters from SSFR test results are compared with design values and to traditional "sudden no-load three-phase short-circuit", Dalton-Cameron and "open stator d-axis transient time constant" methods. The measured three-phase short-circuit current waveforms are compared with the waveforms obtained by simulating the SSFR based machine model with an electromagnetic transient type (EMT-type) software (EMTP [25]).

The first part of this paper briefly recalls synchronous machine theory. The second part presents the SSFR test measurements and machine parameter identification. The comparison with machine parameters obtained using traditional methods and validation with "sudden no-load three-phase short-circuit" oscillograms are presented in the last part.

II. Synchronous Machine

A. Synchronous Machine Equivalent Circuits

The d- and q-axis equivalent circuits of a three-phase synchronous machine is illustrated in Fig. 1. The d-axis rotor circuits are composed of one field winding (F) and two damper windings (D1 and D2). The q-axis rotor circuits are composed of three damper windings (Q1, Q2 and Q3). Although a large number of circuits are used to represent damper effects in machine analysis, a limited number of circuits may be used in power system analysis depending on the type of rotor construction and the frequency range of interest. R_a is the stator resistance; L_{al} is the stator leakage inductance; L_{ad} and L_{aq} are the d- and q-axis stator to rotor mutual inductances, respectively. R_F, R_{D1}, R_{D2}, R_{Q1}, R_{Q2}, R_{Q3} are the resistances and L_{Fl}, L_{D1l}, L_{D2l}, L_{Q1l}, L_{Q2l}, L_{Q3l} are the leakage inductances of the F, D1, D2, Q1, Q2 and Q3 windings. L_{FD1} is the leakage inductance that represents the flux linking F, D1 and D2 windings but not the stator d-axis winding. L_{FD2} is the leakage inductance that represents the flux linking F and D2 windings but not the D1 and stator d-axis windings. v_d, λ_d and i_d are the voltage, flux linkage and current of stator d-axis winding. v_q, λ_q and i_q are the voltage, flux linkage and current of stator q-axis winding.

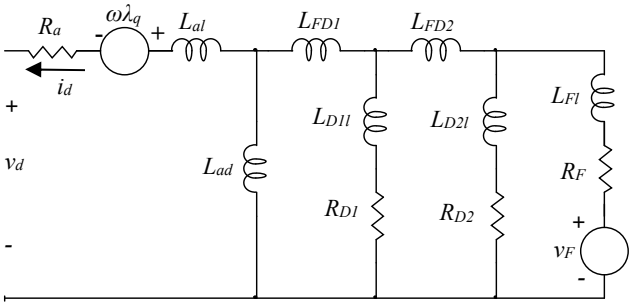

(a) d-axis equivalent circuit

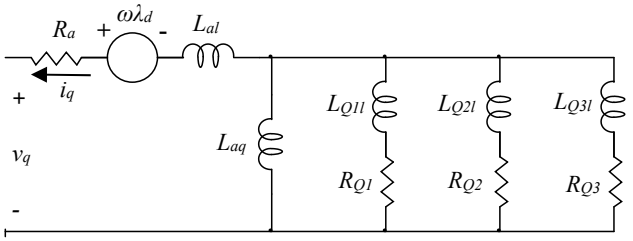

(b) q-axis equivalent circuit

Fig. 1. Synchronous machine equivalent circuits [26].

Table I shows the matrix of rotor structures proposed in the IEEE Standard 1110-2002 [27]. Up to 12 combinations are possible, but only 6 of them are considered. Model 3.3 in Table I corresponds to the equivalent circuit given in Fig. 1. Model selection is usually based on the machine type, study to be performed, user's experience, and available information. The most complex models (such as Model 3.3) usually cannot be used due to lack of data [26], [28]. Model 2.2 and Model 2.1 are widely used to represent cylindrical and SPSMs, respectively. The inductance L_{FD1} is usually omitted [26], [29].

TABLE I
SYNCHRONOUS MACHINE MODELS FOR TRANSIENT STUDIES

	q-axis			
d-axis	*No damper circuit*	*1 damper circuit*	*2 damper circuits*	*3 damper circuits*
Field circuit only	Model 1.0	Model 1.1	Not Used	Not Used
Field circuit + 1 damper circuit	Not Used	Model 2.1	Model 2.2	Model 2.3
Field circuit + 2 damper circuits	Not Used	Not Used	Not Used	Model 3.3

B. Synchronous Machine Operational Parameters

Relations between stator and field quantities can be expressed in the operational form [26]:

$$\lambda_d(s) = G(s)v_F(s) + L_d(s)i_d(s) \quad (1)$$

$$\lambda_q(s) = L_q(s)i_q(s) \quad (2)$$

where $G(s)$ is the stator-to-field transfer function, $L_d(s)$ is the d-axis operational inductance, $L_q(s)$ is the q-axis operational inductance and $s = j\omega$ is the Laplace variable.

For Model 3.3,

$$G(s) = \frac{L_{ad}}{R_F}\frac{(1+sT_{kd1})(1+sT_{kd2})}{(1+sT'_{d0})(1+sT''_{d0})(1+sT'''_{d0})} \quad (3)$$

$$L_d(s) = L_d\frac{(1+sT'_d)(1+sT''_d)(1+sT'''_d)}{(1+sT'_{d0})(1+sT''_{d0})(1+sT'''_{d0})} \quad (4)$$

$$L_q(s) = L_q\frac{(1+sT'_q)(1+sT''_q)(1+sT'''_q)}{(1+sT'_{q0})(1+sT''_{q0})(1+sT'''_{q0})} \quad (5)$$

where $L_d = L_{al} + L_{ad}$; $L_q = L_{al} + L_{aq}$; T'_d, T''_d and T'''_d (T'_q, T''_q and T'''_q) are d-(q-) axis short-circuit transient, subtransient and subsubtransient time constants respectively; T'_{d0}, T''_{d0} and T'''_{d0} (T'_{q0}, T''_{q0} and T'''_{q0}) are d-(q-) axis open-circuit transient, subtransient and subsubtransient time constants, respectively. Definitions of the time constants T_{kd1} and T_{kd2}, and equivalent circuit parameter calculation from the operational parameters can be found in [26]. All values in (3) - (5) are in per-unit.

C. Determination of Synchronous Machine Parameters

Usually, the synchronous machine parameters are determined from the sudden three-phase short-circuit tests on unloaded machines. The test procedures are specified in [1]. These tests provide d-axis transient and subtransient inductances (L'_d, L''_d) as well as transient and subtransient time constants (T'_d, T''_d). These parameters enable the calculation of the d-axis operational inductance $L_d(s)$ for field plus one damper winding rotor structure. As these tests do not include measurement for the field circuit, accurate identification of the field circuit is not possible. Hence, d-axis equivalent circuit for the field plus one damper winding rotor structure can be calculated by assuming the flux linking rotor circuits is equal to that linking the stator, i.e. by omitting L_{FD1}.

It should be noted that these tests do not provide q-axis quantities. Special procedures must be used to derive them (see Appendix F of [1]).

The SSFR test has been developed as an alternative to traditional tests. The operational parameters of the machine given in (1) and (2) can be obtained from SSFR test results. These tests enable to obtain high order equivalent circuits such as Model 3.3 in Table I.

III. SSFR Test Measurements

A. Rotor Positioning

Before SSFR testing, the machine is shut down and electrically isolated. Since the SSFR tests are performed independently for d- and q-axes, it is also necessary to align the rotor to two particular positions with respect to the stator.

Accurate rotor positioning is a challenging task in salient pole machines due to large pole numbers as a small error in mechanical positioning can lead to a significant electrical angle error [1], [8]. In the performed SSFR tests, the rotor positioning is carried out based on [1]. The position at the minimum field voltage was used for the alignment. The measured minimum and maximum voltages are presented in Table II.

TABLE II
MEASURED FIELD VOLTAGES WHILE ROTOR POSITIONING

Axis	Stator rms current (A)	Field voltage	
		Maximum (V)	Minimum (mV)
d	9.1	132.2	252
q	8.2	130	46

B. Measured Functions

Table III shows the test setups for each of the measurable parameters and the main relations derived from each test.

$Z_d(s)$ and $Z_q(s)$ are the direct and quadrature operational impedances as viewed from the armature terminals. The operational inductances are found from

$$L_d(s) = \left(Z_d(s) - R_a\right)/s \quad (6)$$

$$L_q(s) = \left(Z_q(s) - R_a\right)/s \quad (7)$$

The function $sG(s)$ is used instead of $G(s)$. The parameters of the d-axis equivalent circuit shown in Fig. 1.a, can be obtained using the transfer functions $Z_d(s)$ and $sG(s)$.

The q-axis equivalent circuit parameters shown in Fig. 1.b, can be obtained using the operational impedance $Z_q(s)$.

C. Equivalent Circuit Parameters

1) Preliminary Analysis

a) Stator Resistance

The stator resistance given in Table IV is calculated from the measured $Z_d(s)$ and $Z_q(s)$ using

$$R_{a-i} = \lim_{s\to 0}\text{Real}\left[Z_i(s)\right], \quad i = d, q \quad (8)$$

As seen from Table IV, the stator resistance obtained with SSFR measurement is very close to the one obtained with the Kelvin Bridge.

b) Stator Leakage Inductance

The best available estimate is used for the stator leakage inductance. The value supplied by the manufacturer ($L_{al} = 0.27$ p.u.) is used in this paper as recommended in [1] and [27].

TABLE III
STANDARD SSFR TESTS [28]

Test Diagram	Measurement	Relations
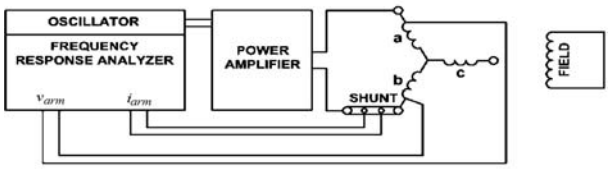	d-axis operational impedance $Z_d(s)$	$Z_d(s) = -\frac{\Delta v_d(s)}{\Delta i_d(s)}\|_{\Delta v_F=0}$ $Z_d(s) = \frac{1}{2}\frac{\Delta v_{arm}(s)}{\Delta i_{arm}(s)} = R_a + sL_d(s)$
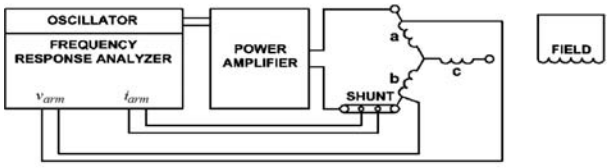	q-axis operational impedance $Z_q(s)$	$Z_q(s) = -\frac{\Delta v_q(s)}{\Delta i_q(s)}\|_{\Delta v_F=0}$ $Z_q(s) = \frac{1}{2}\frac{\Delta v_{arm}(s)}{\Delta i_{arm}(s)} = R_a + sL_q(s)$
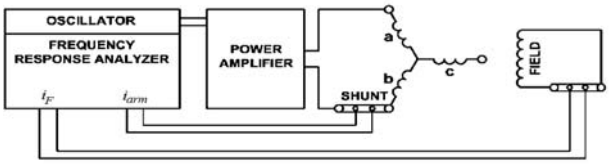	Standstill armature to field transfer function $sG(s)$	$sG(s) = -\frac{\Delta i_F(s)}{\Delta i_d(s)}\|_{\Delta v_F=0}$ $\frac{\Delta i_F(s)}{\Delta i_d(s)} = \frac{\sqrt{3}}{2}\frac{\Delta i_F(s)}{\Delta i_{arm}(s)}$
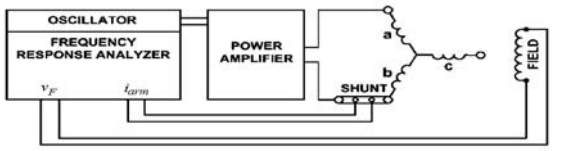	Standstill armature to field transfer impedance $Z_{afo}(s)$	$Z_{afo}(s) = -\frac{\Delta v_F(s)}{\Delta i_d(s)}\|_{\Delta i_F=0}$ $\frac{\Delta v_F(s)}{\Delta i_d(s)} = \frac{\sqrt{3}}{2}\frac{\Delta v_F(s)}{\Delta i_{arm}(s)}$

TABLE IV
STATOR RESISTANCE

Axis	Stator temperature and starting frequency	SSFR resistance at the origin (mΩ)	SSFR value corrected to 25°C (mΩ)	Kelvin Bridge value at 25°C (mΩ)
d	10.5°C at 1 mHz	13.704	14.515	14.410
q	10.7°C at 1 mHz	13.716	14.518	

c) Magnetizing Inductances

The magnetizing inductances are calculated using the low frequency limits of $L_d(s)$ and $L_q(s)$ as shown below.

$$L_{ad}(0) = L_d(0) - L_{al} = 1.028 - 0.27 = 0.758 \text{ p.u.} \quad (9)$$

$$L_{aq}(0) = L_q(0) - L_{al} = 0.865 - 0.27 = 0.595 \text{ p.u.} \quad (10)$$

d) Effective Field to Stator Turns Ratio

The effective field to stator turns ratio N_{af} is calculated using the armature to field transfer impedance $Z_{afo}(s)$ as shown below (see [26] for details).

$$N_{af}(0) = \frac{1}{sL_{ad}(0)} \lim_{s\to 0} Z_{afo}(s) = 7.856 \quad (11)$$

e) Field Resistance

The field resistance referred to the stator side is calculated using the low frequency limits of $L_d(s)$ and $sG(s)$:

$$R_F = \frac{sL_{ad}(0)}{(2/3)N_{af}(0)\lim_{s\to 0}\left[\Delta i_F(s)/\Delta i_d(s)\right]} = 5.896\text{m}\Omega \quad (12)$$

2) Rotor Circuit Parameters

This step consists of choosing the rotor circuit structure and a fitting technique to derive the parameters of equivalent circuits (see Fig. 1) that can match the obtained frequency response.

In this paper, the parameters of Model 3.x and Model 2.x (x represents arbitrary q-axis structure in Table I) are obtained using SSFR test measurements. Maximum likelihood estimation (MLE) [22] is used for fitting. The operational parameters $G(\boldsymbol{\eta}_\mathbf{d}, s)$, $L_d(\boldsymbol{\eta}_\mathbf{d}, s)$ and $L_q(\boldsymbol{\eta}_\mathbf{q}, s)$, expressed in terms of the equivalent circuit parameters, are obtained using the "Symbolic Math Toolbox" in Matlab [30] without any approximation. $\boldsymbol{\eta}_\mathbf{d}$ and $\boldsymbol{\eta}_\mathbf{q}$ are the vectors of the unknown d- and q-axis parameters, respectively.

a) Unknown Parameters

The stator leakage inductance L_{al} is provided by the manufacturer. The effective field to stator turns ratio N_{af}, the magnetizing inductances $L_{ad}(0)$ and $L_{aq}(0)$, and field resistance R_F have been already calculated. The vectors of the unknown parameters for Model 3.3 are

$$\begin{aligned}\boldsymbol{\eta}_\mathbf{d} &= \left[R_{D1}\ \ L_{D1l}\ \ R_{D2}\ \ L_{D2l}\ \ L_{Fl}\ \ L_{FD1}\ \ L_{FD2}\right] \\ \boldsymbol{\eta}_\mathbf{q} &= \left[R_{Q1}\ \ L_{Q1l}\ \ R_{Q2}\ \ L_{Q2l}\ \ R_{Q3}\ \ L_{Q3l}\right]\end{aligned} \quad (13)$$

Depending on the selected machine model, certain parameters in the machine equivalent circuits (see Fig. 1) and in the vector of unknowns (see (13)) are removed. For example, the vector $\boldsymbol{\eta}_\mathbf{d}$ (as well as the d-axis equivalent circuit in Fig. 1.a) does not contain R_{D2}, L_{D2l} and L_{FD2} when Model 2.x is selected.

b) Preliminary Equivalent Circuit Parameters

The initial values of unknown parameters have significant impact on the performance of MLE method [23], [24]. For initializing unknown parameters, $G(s)$, $L_d(s)$ and $L_q(s)$ (see (3) - (5)) are fitted to SSFR measurements using the Least Square (LS) method [31]. As $G(s)$ and $L_d(s)$ have the same denominator, the denominator obtained while fitting $L_d(s)$ is used while fitting the numerator of $G(s)$. The obtained solution is presented in Table V.

TABLE V
INITIAL VALUES OF THE STANDARD TIME CONSTANTS

Parameter	*(s)*	*Parameter*	*(s)*
T_d'''	1.9550E-3	T_q'''	2.4746E-3
T_d''	7.6112E-2	T_q''	6.7759E-2
T_d'	9.3341E-1	T_q'	2.9269E-1
T_{d0}'''	2.1258E-3	T_{q0}'''	2.6628E-3
T_{d0}''	8.5445E-2	T_{q0}''	1.1796E-1
T_{d0}'	1.8643	T_{q0}'	3.0682E-1
T_{kd1}	7.2684E-2		
T_{kd2}	2.1377E-3		

c) Final Equivalent Circuit Parameters

The final values of the unknown rotor circuit parameters are obtained using MLE approach in which the parameter sets ($\boldsymbol{\eta}_\mathbf{d}$ and $\boldsymbol{\eta}_\mathbf{q}$) are determined by maximizing the conditional probability density function of the prediction error for the measured standstill frequency responses. In mathematical terms, MLE seeks the parameter sets $\boldsymbol{\eta}_\mathbf{d}$ and $\boldsymbol{\eta}_\mathbf{q}$, which minimize the log likelihood function $V(\boldsymbol{\eta})$ where [24]

$$V(\boldsymbol{\eta})=\frac{1}{2}\sum_{k=1}^{N}\left[\mathbf{e}^T(\mathrm{k},\boldsymbol{\eta})\,\mathbf{R}^{-1}(\mathrm{k},\boldsymbol{\eta})\,\mathbf{e}(\mathrm{k},\boldsymbol{\eta})\right]+\frac{1}{2}\sum_{k=1}^{N}\log\det\left(\mathbf{R}(\mathrm{k},\boldsymbol{\eta})\right) \quad (14)$$

In (14), N is the number of SSFR measurement data points. For the d-axis, the residual error vector $\mathbf{e_d}$ and its covariance matrix $\mathbf{R_d}$ are obtained as follows:

$$\mathbf{e_d}=\begin{vmatrix}|\mathbf{L_d}|-|\hat{\mathbf{L}}_\mathbf{d}|\\ \angle(\mathbf{L_d})-\angle(\hat{\mathbf{L}}_\mathbf{d})\\ |\mathbf{sG}|-|\mathbf{s}\hat{\mathbf{G}}|\\ \angle(\mathbf{sG})-\angle(\mathbf{s}\hat{\mathbf{G}})\end{vmatrix};\quad \mathbf{R_d}=\frac{1}{N}\sum_{k=1}^{N}\mathbf{e_d}\,\mathbf{e_d}^T \quad (15)$$

where hatted parameters are the estimated parameters. Reader should refer to [22] for the utilized synchronous machine parameter identification method from SSFR tests using MLE method.

It should be noted that the error minimization process gives the priority to $L_d(s)$ at the expense of $sG(s)$. This is done by applying appropriate weighting factors. In addition, the fitting is prioritized between 0.05 and 5 Hz, i.e. the frequency range where most of the grid disturbances take place [4]. The fitting results are presented in Fig. 2 - Fig. 5. Second order model fits adequately the measured data in the range dc to10 Hz whereas third order extends the good fit to 120 Hz. The corresponding d-axis equivalent circuit parameters for Model 3.x and Model 2.x (x represents arbitrary q-axis structure in Table I) are presented in Table VI. Table VI also presents the preliminary d-axis equivalent circuit parameters obtained from the parameters presented in Table V. The presented results in Table VI include the following corrections: substituting the SSFR deduced rotor resistance by the rotor resistance measured with the Kelvin bridge, correcting the rotor resistance for 75^0C operating temperature and replacing the SSFR $L_{ad}(0)$ value by the one obtained from calculated open and short-circuit characteristic curves.

As the SSFR tests are performed using very low currents (30 A in these tests for dc to 20 Hz) compared to rated armature current, the low-level iron nonlinearity cannot be ignored. In other words, the values of iron-dependent inductance measured during SSFR tests will be lower than unsaturated values on the air-gap line. Therefore, $L_{ad}(0)$ derived to match standstill test data must be replaced with the unsaturated L_{ad} value obtained from the open-circuit and short-circuit characteristic curves.

The armature to field transfer impedance $Z_{afo}(s)$ can be be also taken into account while estimating d-axis unknown parameters. However, it is not considered in this paper due to space limitations. It should be also emphasized here that IEEE Standard 115-2009 recommends calculating d-axis parameters considering only $L_d(s)$ and $sG(s)$.

TABLE VI
D-AXIS EQUIVALENT CIRCUIT PARAMETERS IN PER-UNIT

Parameter	*Model 3.x* (dc to 120 Hz)	*Model 3.x* (initial values)	*Model 2.x* (dc to 10 Hz)
L_{al}	2.700E-1	2.700E-1	2.700E-1
L_{ad}	9.200E-1	9.200E-1	9.200E-1
L_{FD1}	-1.468E-1	-1.161E-1	-1.660E-1
R_{D1}	7.460E-2	5.410E-2	8.260E-2
L_{D1l}	1.800	1.482	1.867
L_{FD2}	-1.436	-4.876E-1	---
R_{D2}	50.619	10.239	---
L_{D2l}	30.098	8.252	---
R_F	1.213E-3	1.213E-3	1.213E-3
L_{Fl}	1.946	9.752E-1	5.268E-1

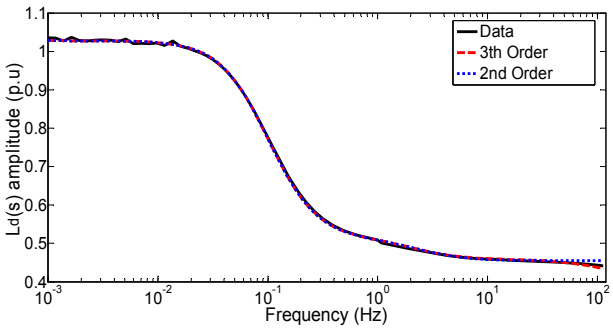

Fig. 2. Measured and fitted $L_d(s)$ amplitude

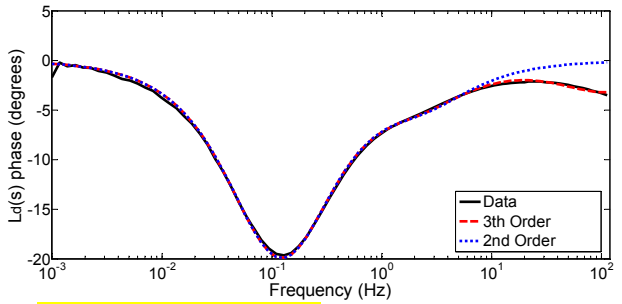

Fig. 3. Measured and fitted $L_d(s)$ phase

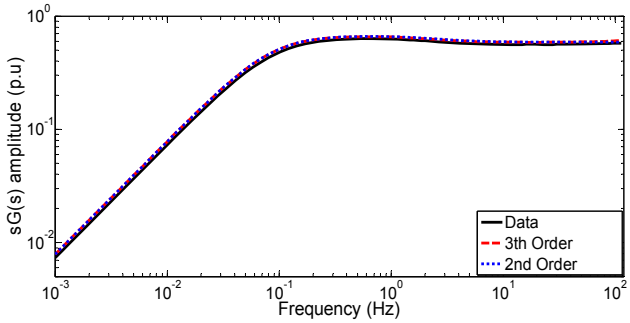

Fig. 4. Measured and fitted $sG(s)$ amplitude

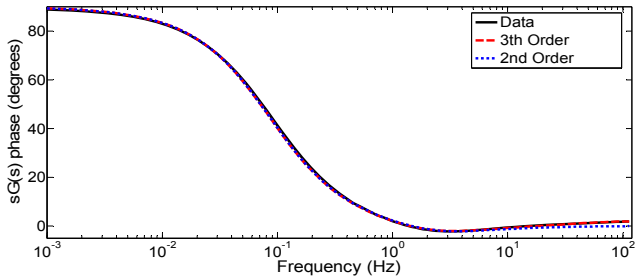

Fig. 5. Measured and fitted $sG(s)$ phase

For the q-axis, the residual error vector $\mathbf{e_q}$ and its covariance matrix $\mathbf{R_q}$ are obtained as follows:

$$\mathbf{e_q} = \begin{vmatrix} |\mathbf{L_q}| - |\hat{\mathbf{L}}_\mathbf{q}| \\ \angle(\mathbf{L_q}) - \angle(\hat{\mathbf{L}}_\mathbf{q}) \end{vmatrix}; \quad \mathbf{R_q} = \frac{1}{N}\sum_{k=1}^{N} \mathbf{e_q}\,\mathbf{e_q}^T \qquad (16)$$

The fitting results for q-axis are given in Fig. 6 and Fig. 7. The first order model permits good match up to 10 Hz which is enough sufficient for most studies. The second order model extends the good fit to 40 Hz while a third order extends it further to 120 Hz. The corresponding equivalent circuit parameters for Model x.3, Model x.2 and Model x.1 (x represents arbitrary d-axis structure in Table I) are presented in Table VII.

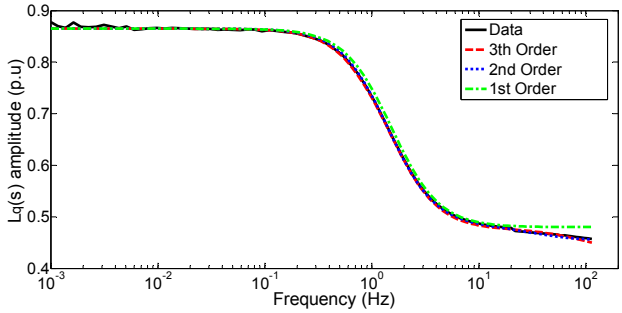

Fig. 6. Measured and fitted $L_q(s)$ amplitude

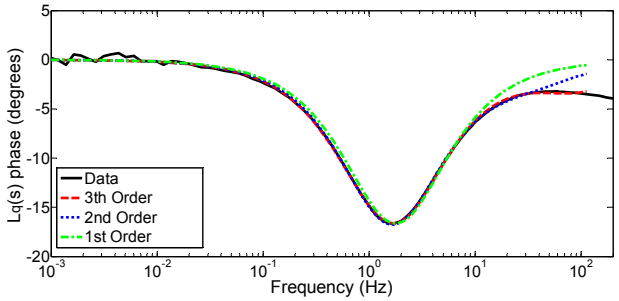

Fig. 7. Measured and fitted $L_q(s)$ phase

TABLE VII
Q-AXIS EQUIVALENT CIRCUIT PARAMETERS IN PER-UNIT

Parameter	*Model x.3* (dc to 120 Hz)	*Model x.2* (dc to 40 Hz)	*Model x.1* (dc to 10 Hz)
L_{al}	2.700E-1	2.700E-1	2.700E-1
L_{aq}	5.950E-1	5.950E-1	5.950E-1
R_{Q1}	1.877E-1	1.904E-2	1.897E-2
L_{Q1l}	13.560	3.340E-1	3.149E-1
R_{Q2}	1.980E-2	8.308E-1	---
L_{Q2l}	3.249E-1	1.294	---
R_{Q3}	1.475	---	---
L_{Q3l}	7.466E-1	---	---

IV. SSFR DATA AND EQUIVALENT CIRCUITS

A. SSFR Data Accuracy

The SSFR measurements at low frequencies provide very high accuracy as the d- and q-axes stator resistances obtained from SSFR measurements are very close to the stator resistance obtained with the Kelvin bridge (see Table IV).

The measured field resistance referred to the stator side was calculated as 5.896 mΩ (see (12)). When this value is referred to rotor side,

$$R_{F-r} = (2/3)\left(N_{af}(0)\right)^2 R_F = 242.60 \text{ m}\Omega \qquad (17)$$

As R_{F-r} includes 100 mΩ current measuring shunt resistance and a supplemental 4.5 mΩ corresponding to the carbon graphite brushes resistance, the actual field resistance value is 138.10 mΩ at 13.5^{0}C. The measured field resistance value using a Kelvin bridge is 143.3 mΩ at 25^{0}C (i.e. equivalent to 136.95 mΩ at 13.5^{0}C).

To the authors' best knowledge, such high accuracy has not been achieved in previous works. For example, the difference between the SSFR and Kelvin bridge measurements is 88% in [11] for the field resistance of a 654 kVA synchronous machine. One reason might be the poor precision of the available instrumentation.

The presented $L_d(s)$ and $L_q(s)$ waveforms also confirm the accuracy of SSFR measurements at low frequencies as there is a clear horizontal asymptote at the origin in both waveforms. It is emphasized that many of those waveforms presented in literature show discrepancies and sometimes a slope instead of a clear horizontal asymptote at the origin.

B. *Magnetic Iron Nonlinearity at Low Excitation*

The iron nonlinearity at low excitation was explained in [5] and also reported in [1]. The obtained $L_{ad}(0)$ value from SSFR measurements is 17.6% less than the one calculated from the open-circuit and short-circuit characteristic curves. In the q-axis, this problem is practically absent as the majority of the flux path is in the air and the impact of iron nonlinearity is not significant. The obtained $L_{aq}(0)$ value from the SSFR measurements is even slightly superior to the design value. In a sharp contrast, the measured $L_{aq}(0)$ is 20% below the design value for a 1.4 MVA hydroelectric machine in [11]. With 10 poles, a rated speed of 720 rpm and a retaining end rings ensuring interpolar damper winding connections, it is suspected that the rotor design is more similar to that of a turbo-generator than to a low speed salient pole machine rotor. This particular rotor design is probably behind iron influence in q-axis for the tested machine in [11].

C. *Equivalent Circuit Elements and Model Order*

The second damper's high resistance and inductance values in Table VI confirm that Model 2.x is sufficient for the tested machine. In the same table, L_{FD1} and L_{FD2} have negative values. This latter result comforts the explanation given in [32], i.e. the mutual flux coupling between rotor circuits is less good than between stator and rotor circuits in salient pole machines.

The Model x.1 is frequently used for salient pole machines. Obtained results confirm that this order reproduces adequately SSFR measurements at frequencies below 10 Hz as shown in Fig. 6 and

Fig. 7. Model x.3 is required to extend the fit to 120 Hz for the tested machine. In a future publication, it will be shown that for large SPSMs with non-continuous damper windings, $L_q(s)$ in the subtransient region highly depends on the quality of electric contact between poles' iron and rotor rim. On machines with such a design, it will be shown that the subtransient $L_q(s)$ signature can change following the runaway test [33].

V. Synchronous Machine Standard Parameters

The synchronous machine characteristics of interest are the effective inductances seen from the terminals of the machine and associated with fundamental frequency currents during sustained, transient, subtransient and subsubtransient conditions. For d-axis (q-axis), these inductances are L_d, L'_d, L''_d and L'''_d (L_q, L'_q, L''_q and L'''_q), respectively. In addition to these inductances, the corresponding time constants, which determine the rate of decay of currents and voltages, form the standard parameters used in specifying synchronous machine electrical characteristics. The standard parameters obtained from SSFR tests are presented in Table VIII in addition to the parameters obtained with classical tests and the manufacturer design values. In Table VIII, the inductances are in per-unit and time constants are in seconds. The data conversion procedures from the standard parameters to the equivalent circuit parameters (or vice versa) can be found in [26].

In Table VIII, T_a is the armature time constant and L_2 is the negative sequence inductance. Their definition and calculation from the equivalent circuit parameters can be found in [26].

TABLE VIII
Standard Parameters

		Measured values at 75°C			
	Design value (at 75°C)	SSFR Tests	2 and 3 phase short-Circuit Tests	Dalton-Cameron	T'_{d0}
T'''_d	--	0.0013	--	--	--
T''_d	0.06	0.06	0.06	--	--
T'_d	1.27	1.25	1.28	--	--
T'''_{d0}	--	0.0015	--	--	--
T''_{d0}	0.07	0.07	--	--	--
T'_{d0}	2.94	2.82	--	--	3.03
L'''_d	--	0.42	--	--	--
L''_d	0.43	0.46	0.45	0.46	--
L'_d	0.49	0.53	0.55	--	--
L_d	1.19	--	--	--	--
T'''_q	--	--	--	--	--
T''_q	--	0.07	--	--	--
T'''_{q0}	--	--	--	--	--
T''_{q0}	0.10	0.12	--	--	--
L'''_q	--	--	--	--	--
L''_q	0.45	0.48	--	0.49	--
L'_q	0.83	0.86	--	--	--
L_q	0.83	0.86	--	--	--
T_a	0.20	0.24	0.25	--	--
L_2	0.44	0.45	0.46	0.47	--

VI. SSFR vs Conventional Tests

Classical tests described in [1] and the manufacturer design values are compared to SSFR parameters in Table VIII. The T'_{d0} column is the open stator d-axis transient time constant test. It is noticed that SSFR parameters obtained at a negligible excitation current level of 0.0091 per-unit are similar to those obtained at rated short-circuit current. SSFR and Dalton-Cameron tests lead to nearly the same values for L''_d and L''_q. The q-axis transient regime is neglected in laminated rotor salient pole machine [26], [29]. Therefore, L_q and L'_q are considered to be equal. Fig. 6, depicts clearly the absence of poles in the transitory region which results in a flat plateau and therefore the same amplitude as L_q.

VII. Model Validation

The "sudden no-load three-phase short-circuit" current waveforms obtained by simulating the SSFR based machine model Model 2.1 in EMT-type software, are compared with measured waveforms in Fig. 8 and Fig. 9. The presented short-

circuit test is the one performed at 50% of rated voltage. It should be noted that Model 3.1 produces similar results with Model 2.1. The presented waveforms in Fig. 8 and Fig. 9 confirm the accuracy of the SSFR based machine model. The differences between the simulated and measured waveforms in stator phase-a current, are mainly due to the drift in frequency during short-circuit.

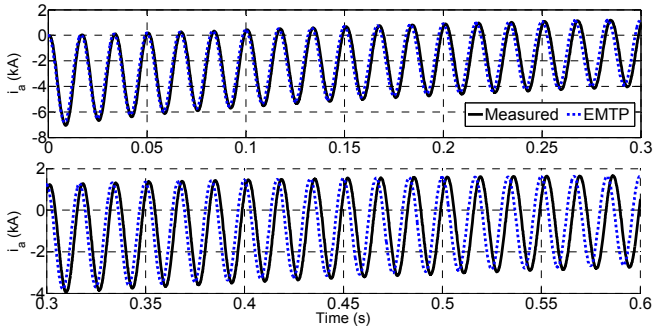

Fig. 8. Sudden no-load three-phase short-circuit stator current (phase-a)

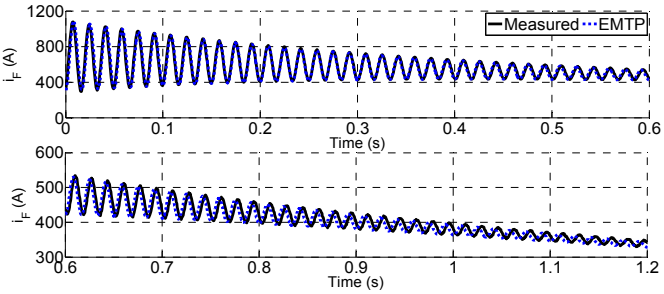

Fig. 9. Sudden no-load three-phase short-circuit field current

VIII. CONCLUSION

This paper contributed to the literature with a detailed SSFR test methodology applied to a large salient pole machine with the objective of improving the requirements and guidance found in the IEEE Standard 115-2009 currently under revision by a working group of the IEEE Electric Machinery Committee. High quality SSFR data are obtained by using an accurate frequency response analyzer and the same constant current in the low frequency range for all measured transfer functions.

These factors resulted in high accuracy in the low frequency region. Stator and rotor resistances deduced from the SSFR test are therefore very close to the values measured by a Kelvin bridge.

As demonstrated for the tested machine, there is no doubt that the SSFR method is as efficient as the standard tests conducted in time-domain. Within the measurement accuracy, the obtained parameters from SSFR tests and traditional methods are close to design values. Moreover, simulations with an EMT-type software produce current waveforms similar to those obtained from the "sudden no-load three-phase short-circuit" tests without any adjustments in the parameters obtained from SSFR tests, which is in sharp contrast with SSFR experiences reported in the literature. Such a positive result is probably to occur, for all machines with d-axis damper winding circuits that are unaffected by rotation. Large salient pole machines are among this category of machines.

REFERENCES

[1] *IEEE Guide: Test Procedures for Synchronous Machines Part I - Acceptance and Performance Testing Part II - Test Procedures and Parameter Determination for Dynamic Analysis*, IEEE Std. 115, 2009.

[2] R. Diggle and J. L. Dineley, "Generator Works Testing. Sudden-Short-Circuit or Standstill Variable-Frequency-Response Method," *Proc. Inst. Elect. Eng. C*, vol. 128, no. 4, pp. 177–182, Jul. 1981.

[3] R. Saunders, "Standstill Frequency-Response Methods and Salient-Pole Synchronous Machines," *IEEE Trans. Energy* Convers., vol. 14, no. 4, pp. 1033–1037, Dec. 1999.

[4] P. L. Dandeno and A.T. Poray, "Development of Detailed Turbogenerator Equivalent Circuits From Standstill Frequency Response Measurements," *IEEE Trans. Power App. and Syst.*, vol. 100, no. 4, pp. 1646-1655, April 1981.

[5] M. E. Coultes and W. Watson, "Synchronous Machine Models by Standstill Frequency Response Tests," *IEEE Trans. Power App. and Syst.*, vol. 100, no. 4, pp. 1480-1489, April 1981.

[6] S. D. Umans, J.A. Malick, and G.L. Wilson, "Modeling of Solid Rotor Turbogenerators. Part II: Example of Model Derivation and use in Digital Simulation," *IEEE Trans. Power App. and Syst.*, vol. 97, no. 1, pp. 278-291, Jan./Feb. 1978.

[7] G. Zafarabadi and E. Amini Boroujeni, "Identification of Generator Parameters from SSFR Test for Montazer-Qaem Powerplant," *43rd International Universities Power Engineering Conference*, Padova, 2008.

[8] P.L. Dandeno et al., "Experience with Standstill Frequency Response (SSFR) Testing and Analysis of Salient Pole Synchronous Machines," *IEEE Trans. Energy Convers.*, vol. 14, no. 4, pp. 1209-1217, Dec. 1999.

[9] C. J. Azuaje and S. Salon, "Standstill Frequency Response Tests on Hydrogenerators at Macagua II Project," invited to the panel session "SSFR Testing and Analysis of Salient-Pole Machines," *IEEE-PES Winter Meeting*, Feb. 4, 1997.

[10] D. Y. Park, H. C. Karmaker, G. E. Dawson, and A. R. Eastham, "Standstill Frequency Response Testing and Modeling of Salient-Pole Synchronous Machines," *IEEE Trans. Energy Convers*., vol. 13, no. 3, pp. 230–236, Sept. 1998.

[11] D. H. Park, "Parameter Identification of Salient-Pole Synchronous Machines Using the SSFR (Standstill Frequency Response) Test," *Master thesis*, Queen's University, Kingston, Canada, 1997.

[12] J. Verbeeck, R. Pintelon, and P. Lataire, "Identification of Synchronous Machine Parameters Using a Multiple Input Multiple Output Approach," *IEEE Trans. Energy Convers.*, vol. 14, no. 4, pp. 909–917, Dec. 1999.

[13] J. Verbeeck, "Standstill frequency response measurement and identification methods for synchronous machines," *Ph.D. dissertation*, Vrije Universiteit, Brussel, Belgium, Jan. 2000.

[14] T. L. Vandoorn, F. M. De Belie, T. J. Vyncke, J. A. Melkebeek and P. Lataire, "Generation of Multisinusoidal Test Signals for the Identification of Synchronous-Machine Parameters by Using a Voltage-Source Inverter," in *IEEE Trans. on Industrial Electronics*, vol. 57, no. 1, pp. 430-439, Jan. 2010.

[15] A. Keyhani, S. Hao, and G. Dayal, "The Effects of Noise on Frequency-Domain Parameter Estimation of Synchronous Machine Models," *IEEE Trans. Energy Convers*., vol. 4, no. 4, pp. 600-607, Dec. 1989.

[16] G. Ahrabian and A. M. El-Serafi, "Identification of the Synchronous Machine Parameters under Magnetic Saturated Conditions using Stand Still Frequency Response Test," in *Proc. Can. Conf. Elect. Comput. Eng*., pp. 545-550, Toronto, Canada, 2001.

[17] S. Rakotovololona, "Mise en Oeuvre et Validation de la Méthode des Réponses en Fréquence à l'Arrêt - Standstill Frequency Response (SSFR) - pour trois générateurs synchrones, " *Master thesis*, Laval University, Nov. 2015.

[18] O. Hernandez-Anaya, T. Niewierowicz, E. Campero-Littlewood, and R. Escarela-Perez, "Noise Impact in the Determination of Synchronous Machine Equivalent Circuits using SSFR Data," *3rd International Conf. on Electrical and Electronics Engineering*, Veracruz, 2006, pp. 1–4.

[19] J. Verbeeck, R. Pintelon, and P. Lataire, "Influence of Saturation on Estimated Synchronous Machine Parameters in Standstill Frequency Response Tests," *IEEE Trans. Energy Convers.*, vol. 15, no. 3, pp. 277–283, Sep. 2000.

[20] J. Bladh, M. Wallin, L. Saarinen and U. Lundin, "Standstill Frequency Response Test on a Synchronous Machine Extended With Damper Bar Measurements," *IEEE Trans. Energy Convers.*, vol. 31, no. 1, pp. 46-56, Mar. 2016.

[21] Solatron 1260A Technical Specifications. Available: http://www.solartronanalytical.com/our-products/potentiostats/Model-1260A.aspx.
[22] A. Keyhani, S. Hao and R. P. Schulz, "Maximum Likelihood Estimation of Generator Stability Constants using SSER Test Data," *IEEE Trans. Energy Convers.*, vol. 6, no. 1, pp. 140-154, Mar. 1991.
[23] I. Kamwa, P. Viarouge, H. Le-Huy and J. Dickinson, "A Frequency-Domain Maximum Likelihood Estimation of Synchronous Machine High-Order Models using SSFR Test Data," *IEEE Trans. Energy Convers.*, vol. 7, no. 3, pp. 525 - 536, Sept. 1992.
[24] A. Keyhani and H. Tsai, "Identification of High-Order Synchronous Generator Models from SSFR Test Data," *IEEE Trans. Energy Convers.*, vol. 9, no. 3, pp. 593-603, Sep. 1994.
[25] J. Mahseredjian, S. Dennetiere, L. Dube, B. Khodabakhchian, and L. Gerin-Lajoie, "On a new approach for the simulation of transients in power systems," Elect. Power Syst. Res., vol. 77, no. 11, pp. 1514-1520, Sep. 2007.
[26] U. Karaagac, J. Mahseredjian, and J. A. Martinez-Velasco, "Synchronous machines," in Power System Transients: Parameter Determination. Boca Raton, FL: CRC Press/Taylor & Francis, Oct. 2009, ch. 5, p. 103.
[27] *IEEE Guide for Synchronous Generator Modeling Practices and Applications in Power System Stability Analysis*, IEEE Std. 1110, 2002.
[28] J.A. Martinez, B. Johnson, and C. Grande-Moran, "Parameter determination for modeling system transients. Part IV: Rotating machines," *IEEE Trans. on Power Delivery*, 20(3), 2063-2072, Jul. 2005.
[29] P. Kundur, *Power System Stability and Control*. New York, USA: McGraw-Hill,1994.
[30] Symbolic Math Toolbox User's Guide. The MathWorks, Inc. Sep. 2011.
[31] D. Marquadt, "An Algorithm for Least Squares Estimation of Non-Linear Parameters," *SIAM Journal*, Vol. 11, no. 22, pp. 431-444, 1963.
[32] I. M. Canay, "Causes of Discrepancies on Calculation of Rotor Quantities and Exact Equivalent Diagrams of the Synchronous Machine," *IEEE Trans. Power App. Syst*., vol. 88, no. 7, pp. 1114–1120, Jul. 1969.
[33] E. Desbiens, D. Proulx, N. Caron and G. Proulx, "Prototype Efficiency and Runaway Tests on 223 MW Kaplan and 116 MW Propeller Turbines,"*International Conf. on Hydropower*, Beijing, China, Oct. 1996.